A Cross-sectional Profile Based Model for Stripline Conductor Surface Roughness

Shaohui Yong^{#1}, Victor Khilkevich^{#2}, Yuanzhuo Liu^{#3}, Ruijie He^{#4}, Yuandong Guo^{#5}, Han Gao⁺⁶, Scott Hinaga⁺⁷, Darja Padilla⁺⁸, Douglas Yanagawa⁺⁹, Jun Fan^{#10}, James Drewniak^{#11}

*EMC Laboratory, Missouri University of Science and Technology, Rolla, MO. 65401 USA

*Cisco Systems, Inc, San Jose, CA. 95134 USA

1sy2m5, 2khilkevichy, 3liuyuanz, 4rhrg8, 5ydggdd, 10jfan, 11drewniak@mst.edu

6hgao2, 7shinaga, 8darja, 9yanagawa@cisco.com

Abstract—As the data rate of high-speed digital systems is getting higher, the conductor loss can no more be modeled assuming perfectly smooth conductor surfaces for even the smoothest foils available. The Huray model, based on the analytical calculation of the additional loss due to the scattering/absorption from conductive spheres on a smooth plane, has been presented to account for this issue. However, in practice it is very difficult to determine the parameters of the model. A modeling approach relating the parameters of the model to the conductor roughness profiles is needed. In this paper an investigation of the scattering by metal hemispheres, including their interaction, is performed. A method is brought up to estimate the multi-level physical model's parameters using the scanning electron microscope (SEM) or optical cross-sectional profile imaging. Accurate modeling of the frequency-dependent conductor loss is achieved.

Index Terms—Skin effect, surface roughness, striplines, printed circuit boards, signal integrity

I. INTRODUCTION

Frequency-dependent conductor loss in one of the most important factors for high-speed signal integrity (SI) design. The additional conductor loss due to foil surface roughness is no longer negligible [1-4].

To account for this issue, the empirical surface roughness correction factor was brought up by Hammerstad [5]. However, its accuracy breaks down for frequencies above 5GHz or for rough foil with RMS roughness level above $2\mu m$ [6].

In recent years, the Huray model [7-11], assuming certain conductive structures (pyramidal stacked spheres) on a smooth surface, has gained popularity. Good correlation with measurement results for frequencies up to 50GHz has been shown. However, determining the model parameters has always been a problem. To implement the Huray model, empirical estimation or fitting is often required for two reasons. Firstly, the diameter and number of spheres "inside" the pyramidal stacks are not observable by scanning electron microscope (SEM). Secondly, the Huray model assumes no interaction among the stacked spheres. The spheres shielded or hidden beneath other spheres are supposed to account for less loss than the spheres fully exposed to the wave front. However, for Huray model the loss of the pyramidal stack is calculated by the superposition of power absorbed and scattered from each sphere completely exposed to the incident wave. Thus, theoretically it is questionable that an accurate Huray model

can be built by extracting parameters only through observing SEM images. Practically it means that the set of model parameters needs to be obtained by fitting and tuning the Huray model.

To get rid of the parameters fitting and tuning process, the authors would like to use the idea of multi-level hemispherical model [12] [13]. This model extends the hemispherical model [14] by stacking smaller spheres on top of bigger ones. It shows the potential of utilizing geometrical information to establish the parameters for modeling, since the dimensions of the bigger and smaller spheres might be determined by observing the SEM or optical cross-sectional images. Compared to the parameters tuning approach shown in [12], the proposed method models the interactions among the spheres and the fitting process based on measured insertion loss is no longer needed.

In Section II, the traditional modeling with uniform spheres is analyzed to present the impact from the sphere size to the frequency-dependence of surface roughness correction factor. Section III provides the investigations of the interaction among the smaller and bigger spheres for a typical multi-level surface roughness model. Validations are shown in Section IV using 3D full-wave simulated striplines and a fabricated printed circuit board (PCB).

II. FOIL ROUGHNESS MODELLING WITH UNIFORM SPHERES

Before introducing the proposed modeling approach, we would like to take a look at derivation of surface roughness correction factor and introduce some necessary parameters. As Fig.1 illustrates, the rough surface is modeled by adding spheres to a smooth conductive plane. The incident plane wave's Poynting vector is expressed as [14, (26)]:

$$S = \frac{1}{2}|E_0| \cdot |H_0| = \frac{1}{2}\eta |H_0|^2 \qquad (1)$$

where $|E_0|$ and $|H_0|$ are the magnitude of the magnetic and electric field. The impedance is defined using $\eta = \sqrt{\mu_0/\varepsilon_0\varepsilon_r}$.

The total cross-section of a sphere (σ_{total}) is the superposition of scattering (σ_{sca}) and absorption cross-section (σ_{abs}) [11, (10.62)]:

$$\sigma_{total} = \sigma_{sca} + \sigma_{abs} \tag{2}$$

As [8, Fig.18] demonstrated, within the bandwidth from 1MHz to 100GHz, scattering is almost negligible compared to absorption ($\sigma_{sca} \ll \sigma_{abs}$) for the spheres with radius smaller than 1 μ m. Thus, we assume that the total cross-section of the

sphere is equal to its absorption cross-section ($\sigma_{total} \approx \sigma_{abs}$). With known number of uniform spheres (N) and under the assumption of no interaction between the spheres, the loss due to absorption is calculated using:

$$P_{abs} = N \cdot S \cdot \sigma_{abs} \tag{3}$$

In addition to power absorbed by the spheres, the loss due to the smooth conductor surface (P_{smooth}) needs to be taken into account. The total power loss of the rough conductor (P) is expressed therefore as:

$$P = P_{smooth} + P_{abs}$$

= $P_{smooth} + N \cdot S \cdot \sigma_{abs}$ (4)

The power loss of a lossy conductor plate (P_{smooth}) with area equal to A_{smooth} is [14, Equ. (31)]:

$$P_{smooth} = \frac{\mu_0 \cdot \omega \cdot \delta}{4} \cdot |H_0|^2 \cdot A_{smooth}$$
 (5)

where $\delta = 1/\sqrt{f\sigma\pi\mu_0}$ is the skin depth (for a non-magnetic conductor), σ is the conductivity of the conductor, and μ_0 is the permeability of free space. Typically to account for the additional power loss due to surface roughness, the resistive surface roughness correction factor (K), relating the total power loss to the loss due to the smooth conductor, is defined [8, Equ. (9)]:

$$K = \frac{P}{P_{smooth}} \quad (6)$$

By inserting (1), (4) and (5) into (6), K is expressed as:

$$K = 1 + \frac{2 \cdot \eta \cdot N}{\mu_0 \cdot \omega \cdot \delta \cdot A_{smooth}} \cdot \sigma_{abs} \quad (7)$$

The absorption cross-section (σ_{abs}) of an electrically small sphere of radius a and skin depth δ can be calculated [8, Equ. (6)] as:

$$\sigma_{abs} \approx \frac{3\pi k \delta a^2}{1 + \frac{\delta}{a} + \frac{\delta^2}{2a^2}}$$
 (8)

where $k=2\pi/\lambda$, $\lambda=c\cdot (f\sqrt{\varepsilon_r})^{-1}$, c is the speed of light and ε_r is the dielectric permittivity. Notice that the surface roughness correction factor expressed by (7) is independent of the dielectric material property because ε_r is canceled out by the product of $\eta=\sqrt{\mu_0/\varepsilon_0\varepsilon_r}$ and σ_{abs} presented by (8).

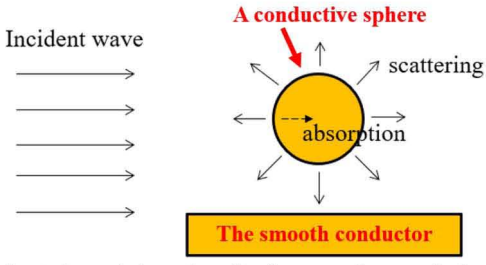


Fig.1. Scattering and absorption of a plane wave by a conducive sphere

The authors would like to point out that the frequency-dependence of absorption cross-section (σ_{abs}), which is the critical factor to determine the surface roughness correction factor (K), is dependent on the sphere radius (α) due to (8). As (7) demonstrates, the number of balls (N) and smooth conductor area (A_{smooth}) only scale the frequency-dependent part of (7). To illustrate this, two examples are created with sphere radius (α) equal to 0.63 μ m and 4.0 μ m, and the corresponding absorption cross-sections are calculated using

(8) assuming air dielectric substrate. As Fig.2 shows, the smaller sphere with $a=0.63\mu m$ leads to a more 'linear' absorption cross-section, while the larger sphere's absorption cross-section tends to bend-down as frequency goes up.

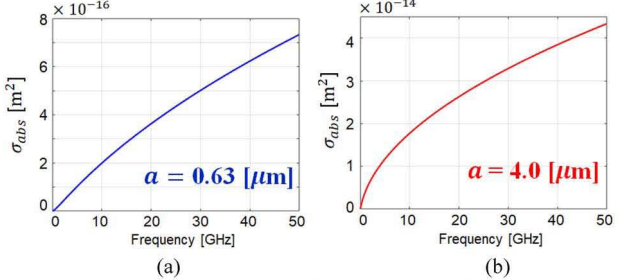


Fig.2. Absorption cross-section (σ_{abs}) of a sphere with radius equal to $0.63\mu m$ (a) and $4.0\mu m$ (b)

III. MULTI-LEVEL SURFACE ROUGHNESS MODEL

To observe the foil surface roughness, a cross-section sample of the stripline is removed from a fabricated PCB, and encapsulated in an epoxy-based compound to make the cross-section of the copper layer of interest perpendicular to the plane of view. To remove the scratches or mechanical damage caused by the cutting, the surface to be viewed is polished with sand paper and diamond polishing compound until the metal surfaces are shiny and no obvious scratches on the surfaces can be observed using an optical microscope. According to the SEM image of the cross-section sample shown in Fig.3, we can observe that the conductor surface has a fractal-type structure. It can be noted that the first-order protrusions on the trace surface are relatively large features with size close to 1-2 µm while small second-order protrusions have sizes from 0.1 to 0.6 μ m. This is quite close to the geometries considered in [12] [13] calling for the multi-level models for roughness.

The multi-level roughness modeling was first suggested in [12]. As Fig.4 illustrates, the first order protrusions are placed on the flat and smooth surface and the second-order protrusions are placed on the surface of the first-order protrusion.

According to an idea of the additive multi-level roughness modeling shown in [13, Equ. (11)], the expression for the uniform spheres (3) can be easily extended to the multi-level structure assuming no interaction between the spheres. The two-level model's absorption loss is calculated using the numbers of first-order and second-order protrusions (N_1, N_2) and their absorption cross-sections $(\sigma_{abs1}, \sigma_{abs2})$:

$$P_{2level} = S \cdot (N_1 \cdot \sigma_{abs1} + N_2 \cdot \sigma_{abs2}) \tag{9}$$

The absorption cross-sections $(\sigma_{abs1}, \sigma_{abs2})$ can be calculated using (8) for known first- and second-order hemisphere radii (a_1, a_2) . Notice that the σ_{abs} of a hemisphere is calculated using the σ_{abs} of a sphere divided by two. The two-level surface roughness correction factor is derived by extending (7):

$$K_{2level} = 1 + \frac{\eta \cdot (N_1 \cdot \sigma_{abs1} + N_2 \cdot \sigma_{abs2})}{\mu_0 \cdot \omega \cdot \delta \cdot A_{smooth}} \tag{10}$$

According to the frequency-dependence analysis illustrated by Fig.2, the second-order protrusion contribute with a more 'linear' term, providing more degrees of freedom compared to the first-order model (7). Notice that (9) is based on the assumption of no interaction among the spheres. However, as we mentioned in the introduction section, the sphere shielded or hidden beneath other spheres are supposed to contribute less loss than the sphere fully exposed to the wave. To relate the parameters of the roughness model to the geometry, interaction among spheres should be taken into account.

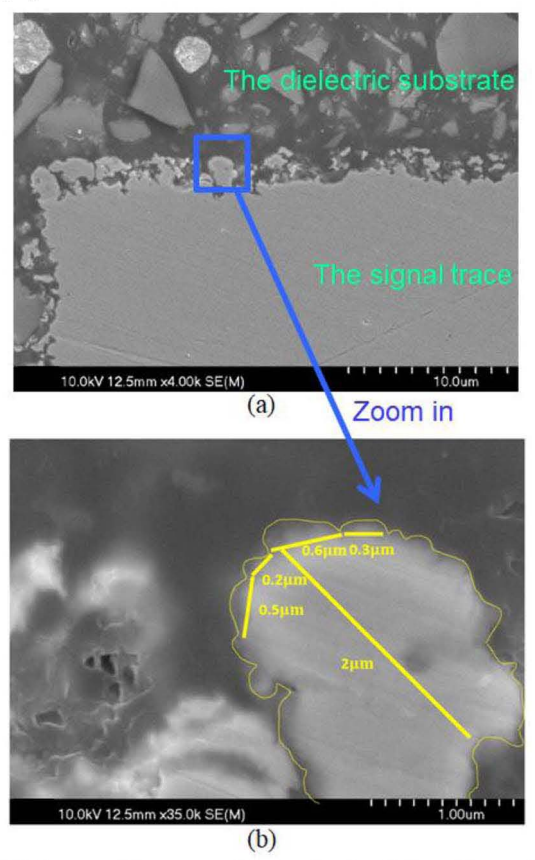


Fig.3. SEM images of the cross-section sample of a stripline with magnification equal to 4K (a) and 35K (b).

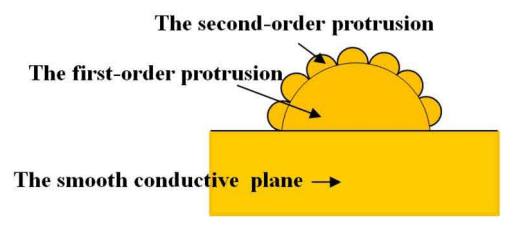


Fig.4. Two-level structure for surface roughness modeling.

To investigate the problem, a two-level surface roughness 3D model is created with one first-order sphere (radius $a_1 = 1.9 \mu \text{m}$) and second-order spheres (radius $a_2 = 0.46 \mu \text{m}$; number $N_2 = 92$) surrounding the first-order sphere as Fig.5 shows. Using the CST MoM solver, the absorption cross-sections of the two-level roughness model (σ_{2level}), first order sphere (σ_1) and the second order sphere (σ_2) are calculated. By comparing the actual cross-section of the two-level structure σ_{2level} to the superposition of the cross-sections of the structure elements $\sigma_1 + N_2 \sigma_2$ presented in Fig.6 it is obvious that the superposition severely overestimates the total cross-section (green dashed curve vs. the solid red one). This is easy to explain by non-uniform distribution of

energy on the surface of the structure (see numerical examples in the next section) which leads to different contributions for different second-order spheres. To account for this effect, we propose to add a compensation factor (k_n) to the superposition formula:

$$\sigma_{\text{2level}} = \sigma_1 + k_n \cdot N_2 \cdot \sigma_2. \tag{11}$$

The coefficient k_nN_2 can be understood as the effective number of the second-order protrusions. By tuning the value of the compensation factor it is possible to approximately match the actual $\sigma_{2\text{level}}$ curve (see Fig.5 – black dashed curve). The value of the compensation factor best fitting the actual cross-section curve was estimated as 0.33.

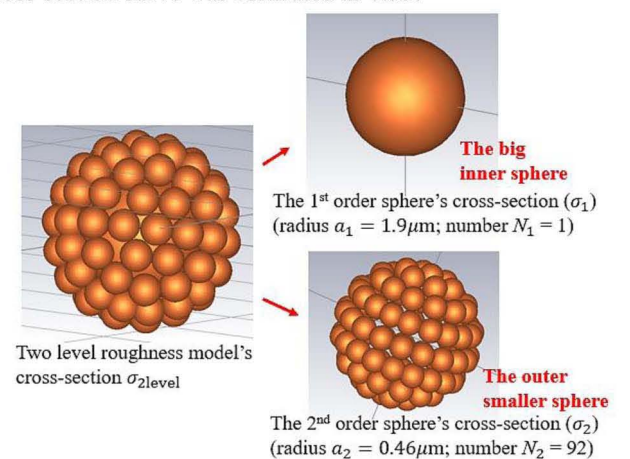


Fig.5. 3D CST two-level model consisting of one inner first-order sphere and many second-order spheres.

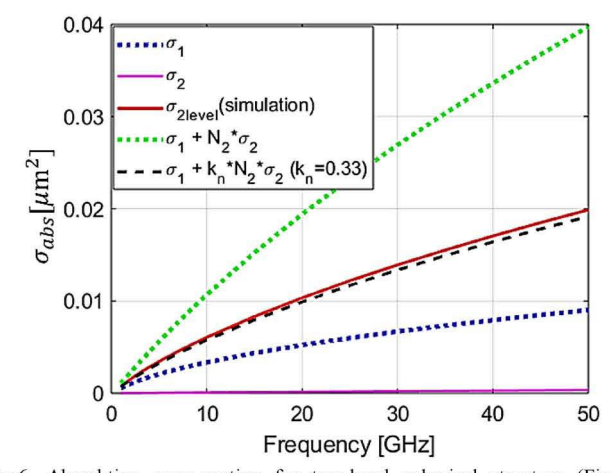


Fig.6. Absorbtion corss-section for two-level spherical structure (Fig.5). Comparison of actual and calculated curves.

To test the robustness of the proposed approximation approach, the authors modeled the first-order protrusion using a cone as Fig.7 shown. The absorption cross-section of the inner cone (σ_1) and outer spheres (σ_2) are calculated by CST. The $\sigma_{2\text{level}}$ is modeled using (12) with $k_n=0.33$. Good match between the modeled and simulated $\sigma_{2\text{level}}$ is shown in Fig.8. This result means that the estimated compensation factor is weakly sensitive the shape of the first-order protrusions.

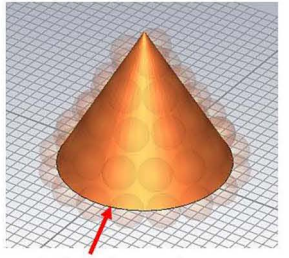
By introducing the compensation factor k_n the final formula for the surface roughness correction factor (K_{2level}) can be written by modifying (10):

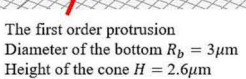
$$K_{2level} = 1 + \frac{\eta \cdot (N_1 \cdot \sigma_{abs1} + k_n N_2 \sigma_{abs2})}{\mu_0 \cdot \omega \cdot \delta \cdot A_{smooth}}$$

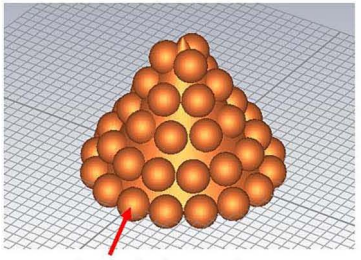
$$= \left(1 + \frac{\eta N_1 \sigma_{abs1}}{\mu_0 \omega \delta A_{smooth}}\right) + \left(1 + \frac{\eta k_n N_2 \sigma_{abs2}}{\mu_0 \omega \delta A_{smooth}}\right) - 1$$

$$= K_1 + K_2 - 1$$

where the total number of the first-order protrusions is N_1 , and the compensated total number of second-order protrusions is $k_n N_2$. K_1 and K_2 are the surface roughness correction factors for the first- and second-order protrusions expressed in the form of (7).







The second order protrusions Radius of the sphere $r = 0.3 \mu \text{m}$ Number of spheres N = 47

Fig. 7. 3D CST two-level surface roughness model consisting of one inner cone and many second-order spheres .

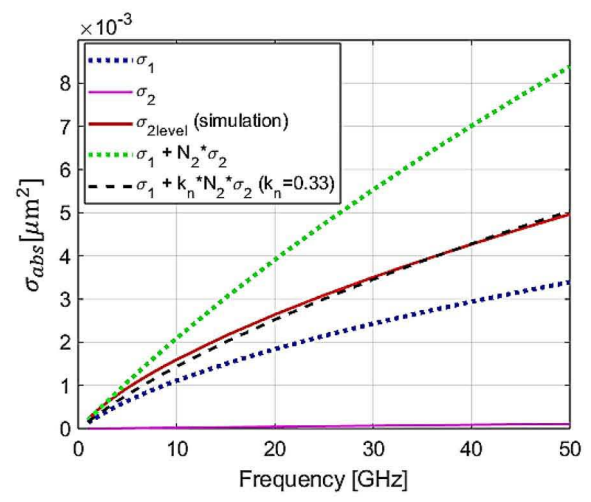


Fig.8. Absorbtion corss-section for two-level conical structure (Fig.7). Comparison of actual and calculated curves.

IV. VALIDATIONS

A. Numerical validations based on 3D simulations

To illustrate the feasibility and accuracy of the proposed method, a 3D model of a transmission line is created and illustrated in Fig.9. The wave propagates from one port to another port (the ports are illustrated by the red surfaces) with vertical electrical field vector. To enforce TEM wave, the upper reference plane is assigned as PEC and the lower singnal trace is assigned with copper. The dielectric substrate is air. The two sides perpendicular to the propagation direction are perfect magnetic walls (tangential magnetic field at the sides is zero). The per-unit-length (PUL) attenuation factors (the real-part of the solver-calculated propagation constant) of the rough line (α_{rough}) and the smooth copper slab (α_{smooth}) are calculated

by the CST frequency-domain solver models shown by Fig.9 (a) and (b).

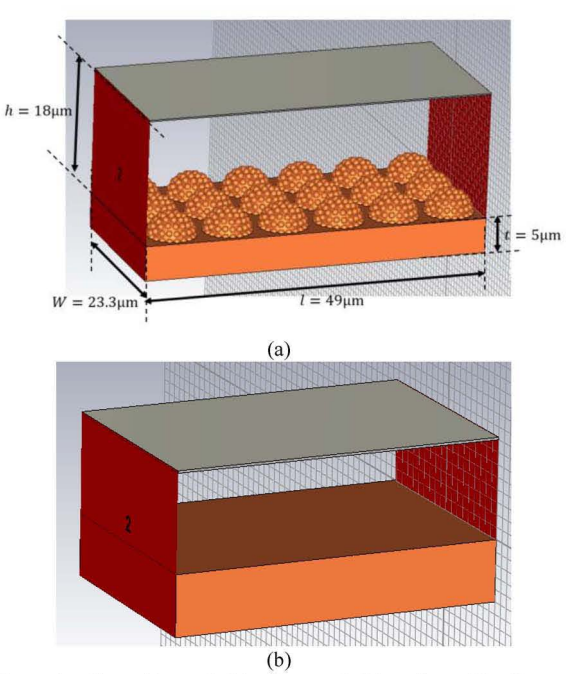


Fig.9. Transmion line with rough (a) and smooth (b) surfaces. The first-order proturtions are modeled using bigger hemispheres with radius $a_1=3\mu m$, and the total big hemisupere number $N_1=18$. The second-order protrusions are modeled using smaller hemispheres with radius $a_2=0.5\mu m$, and the total small hemipshere number $N_2=114$.

Using the proposed approach illustrated by (12), the first and second order protrusion correction factor (K_1, K_2) , and the total two-level surface roughness correction factor (K_{2level}) are calculated using known geometry information and illustrated in Fig.10 (a). It can be observed that the K_2 has more 'linear' frequency-dependence and contributes more to K_{2level} as frequency goes up. Since the dielectric substrate is air, there is no dielectric loss. For practical low-loss transmission lines with $R \ll \omega L$ and $G \ll \omega C$, the attenuation factor can be calculated as:

$$\alpha \approx \frac{1}{2}R\sqrt{\frac{C}{L}} + \frac{1}{2}G\sqrt{\frac{L}{C}},$$
 (13)

where R, L, G, and C are the PUL parameters of the transmission line. Thus, since in the air-filled line G = 0, the attenuation factors of the models in Fig.9 is proportional to the resistance, and the surface roughness correction factor can be used to correct the attenuation factor directly.

By multiplying α_{smooth} by K_{2level} , the modeled α_{rough} is calculated. According to Fig.10 (b), the modeled and simulated α_{rough} can achieve a good match with an error below 5%. The surface power loss density on the line conductor is also calculated in CST. According to Fig.11, it can be seen that the power loss is not distributed on protrusions evenly. Instead, most of the power is lost at the 'crests' of the first-order protrusions, causing certain second-order protrusions to contribute more than others, which implies that the interaction compensation factor (k_n) brought up by the authors is necessary.

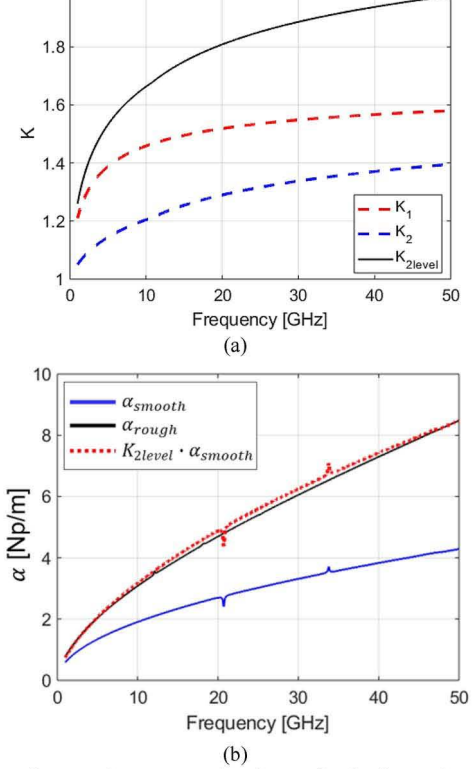


Fig.10. (a) surface roughness correction factors for the first and second order protrusions and the the total two-level model. (b) comparision between the simulated and modeled PUL attenuation factors.

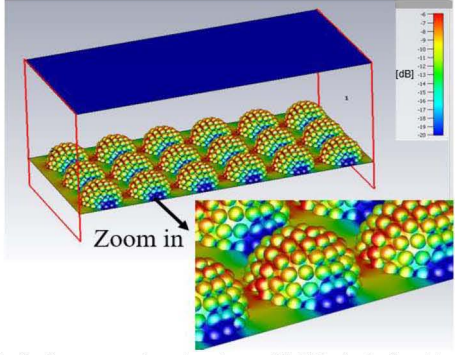


Fig.11. Surface power loss density at 35 GHz (calculated by CST)

B. Modeling using measured data

Let us apply the proposed approach to a differential stripline pair on a fabricated PCB. Using known geometrical information of the stripline [4, Fig.8-9], the smooth PUL resistance (R) is calculated by a 2D solver. After 2X-Thru [16-18] de-emebdding of the 1.3-inch thru line and 16-inch total line, the dielectric material's properties were extracted using the methodology described in [3][4] and presented in Fig. 12. A combination of the optical [16] and SEM microscopy (Fig. 3) is used to determine the parameters of the model. The optical imaging is used primarily to determine the size of the first order protrusions by examining the cross-section profile presented in Fig.13 according to [19]. The radius of the first-order protrusions was set equal to averaged height of the cross-section variations, which, in turn was estimated as 2 μ m.

The radius of the second-order protrusions was estimated as 0.2 μ m by examining Fig.3.

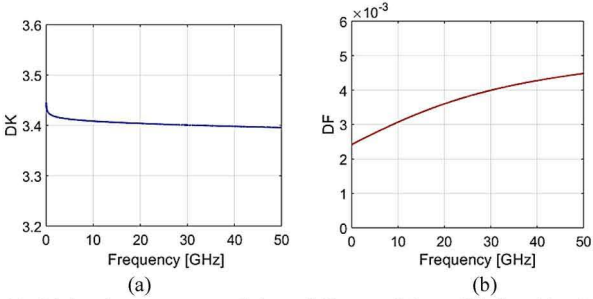


Fig.12. Dielectric parameters of the stripline used for validation (a) relative permittivity (DK). (b) dielectric loss tangent (DF)

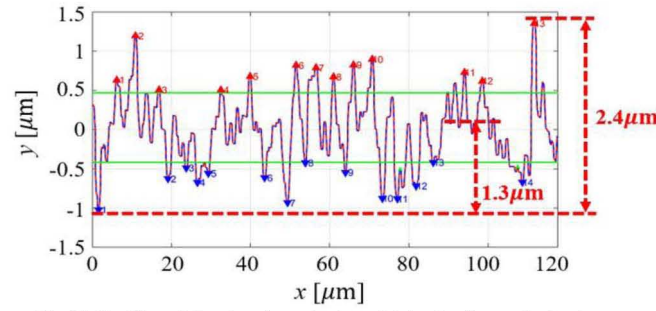


Fig. 13. Profiles of the signal conductors obtained using optical microscopy.

The length of the profile (l_p) is obtained by calculating the length of the curve shown in Fig. 13. Using the assumption of equivalent area, the number of first of-order protrusions (N_1) is calculated using the ratio between the total surface area of the first-order hemispheres (S_{1st}) and one first-order hemisphere's surface area $(S_{1st.0})$:

$$N_1 = \frac{S_{1st}}{S_{1st,0}} = \frac{\frac{2}{\pi} \cdot (l_p)^2}{2\pi (r_1)^2}$$
 (14)

Assuming that the superposition of all second-order spheres' largest cross-sectional areas (A_{2nd}) is equal to the surface area of the first-order sphere (S_{1st}) , the number of second order spheres is calculated:

$$N_2 = \frac{S_{1st}}{A_{2nd}} = \frac{\frac{2}{\pi} \cdot (l_p)^2}{\pi (r_2)^2}$$
 (15)

According to Fig.13, the width of the profile sample is $w=120\mu\text{m}$. The smooth conductor area is calculated assuming a square tile with length equal to w. Thus, $A_{smooth} = w^2$.

The surface roughness correction factors calculated using (12) are illustrated in Fig.14 (a), and the transmission line attenuation factors calculated using the one- and two-level models are shown in Fig. 14 (b) and (c). The measured attenuation factor is obtained using [4, (18)]. It can be observed that the frequency-dependence of the attenuation factor modeled with only the first-order protrusions is not correct. Even after tuning for the number of spheres or area size, the curve can only be scaled, giving good agreement either at low or high frequencies, but not in the entire frequency range. While by using the two-level model as Fig.14 (c) demonstrates, the results can be significantly improved.

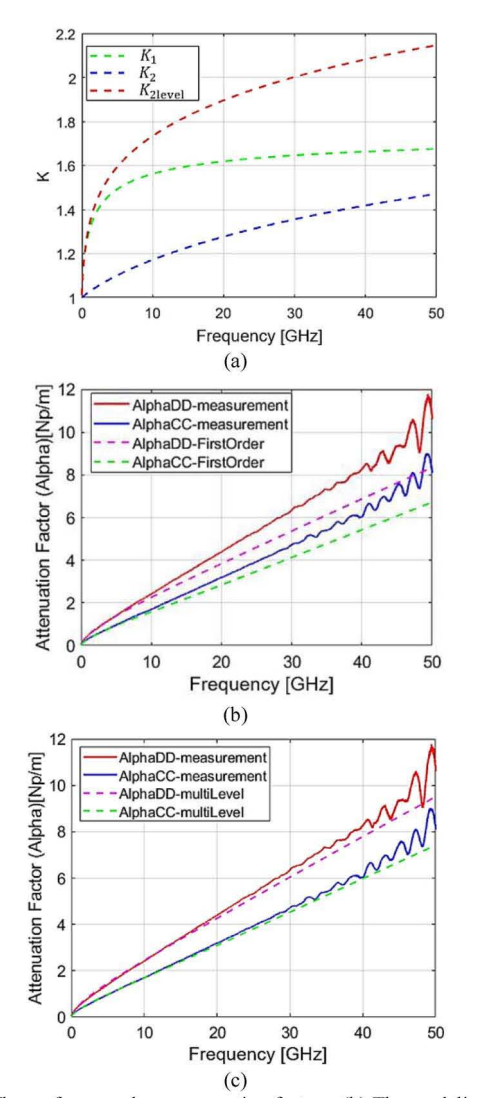


Fig.14. (a) The surface roughness correction factors; (b) The modeling results only using the first-order protrusion correction factor (K_1) ; (c) The modeling results using the two-level correction factor $(K_{2\text{level}})$

V. CONCLUSION

Observation of SEM images of fabricated striplines suggest that the multi-level surface roughness model has a potential to improve accuracy of surface roughness modelling. By introducing a factor to compensate the interaction effect among the first and second order protrusions (spheres), the absorption cross-section of the multi-level roughness structure can be estimated relatively easily.

Compared to the one-level modeling approach, the proposed approach can provide results with more accurate frequency-dependence by introducing the bigger and smaller spheres with different absorption cross-section. The parameters of the model can be relatively easily determined from the SEM and optical cross-sectional images, allowing to avoid complicated model parameter tuning process.

ACKNOWLEDGMENT

This paper is based upon work supported partially by the National Science Foundation under Grant No. IIP-1916535.

REFERENCES

- [1] X. Guo, H. Gao, G. Shen, Q. Liu, V. Khilkevich, J. Drewniak, S. De, S. Hinaga, D. Yanagawa, "Design methodology for behavioral surface roughness model", in *Proc. IEEE Int. Symp. EMC*, Ottawa, 2016, pp. 927-931
- [2] S. Jin, X. Fang, B. Chen, H. Gao, X. Ye, J. Fan, "Validating the transmission-line based material property extraction procedure including surface roughness for multilayer PCBs using simulations", in *Proc. IEEE Int. Symp. EMC*, Ottawa, CN, USA, Jul. 25–29, 2016, pp. 472–477.
- [3] S. Yong, Y. Liu, H. Gao, B. Chen, S. De, S. Hinaga, D. Yanagawa, J. Drewniak, V. Khilkevich, "Dielectric Dissipation Factor (DF) Extraction Based on Differential Measurements and 2-D Cross-sectional Analysis", in *Proc. IEEE Int. Symp. EMC*, Long Beach, CA, USA, 30 Jul-3, 2018, pp. 217-222.
- [4] S. Yong, V. Khilkcvich, Y. Liu, H. Gao, S. Hinaga, S. De, D. Padilla, D. Yanagawa, J. Drewniak, "Dielectric Loss Tangent Extraction Using Modal Measurements and 2-D Cross-sectional Analysis for Multilayer PCB", *IEEE Trans. Electromagn. Compat.*, Early Access
- [5] E. Hammerstad and O. Jensen, "Accurate Models for Microstrip Computer-Aided Design," in *IEEE MTT-S Intl. Microwave Symposium Digest*, Washington, DC, 1980.
- [6] S. Hall and H. Heck, "Advanced Signal Integrity for High-Speed Digital Designs", Wiley-IEEE press, 2009.
- [7] J. E. Bracken, "A Causal Huray Model for Surface Roughness", DesignCon 2012
- [8] P. G. Huray, O. Oluwafemi, J. Loyer, E. Bogatin, X. Ye, "Impact of Copper Surface Texture on Loss: A Model that Works", *DesignCon* 2010
- [9] P. G. Huray, S. Hall, S. Pytel, F. Oluwafemi, R. Mellitz, D. Hua, P. Ye, "Fundamentals of a 3-D 'snowball' model for surface roughness power losses," in Proc. IEEE Workshop Signal Propag. Interconnects, Genova, Italy, May 2007, pp. 121–124.
- [10] E. Bogatin, D. DeGroot, P. G. Huray, Y. Shlepnev, "Which one is better? Comparing Options to Describe Frequency Dependent Losses", *DesignCon 2013*
- [11] Jackson, J. D., "Classical Electrodynamics", 3rd edition. Wiley, New York, 1999.
- [12] Y. Chu, "Method for modeling conductor surface roughness", US Patent#8527246.
- [13] Y. Shlepnev, "Unified approach to interconnect conductor surface roughness modelling", in 2017 IEEE 26st Conference on Electrical Performance of Electronic Packaging and Systems (EPEPS2017), San Jose, CA
- [14] S. Hall, S. G. Pytel, P. G. Huray, D. Hua, A. Moonshiram, G. A. Brist, and E. Sijercic "Multigigahertz Causal Transmission Line Modeling Methodology Using a 3-D Hemispherical Surface Roughness Approach", *IEEE Trans. Microw. Theory Tech.*, vol. 55, no. 12, Dec. 2007, pp. 2614 2624
- [15] D. M. Pozar, "Microwave Engineering". Fourth Edition, John Wiley & Sons, Inc, 2012
- [16] Q. Huang, J. Li, J. Zhou, W. Wu, Y. Qi, and J. Fan, "De-embedding method to accurately measure high-frequency impedance of an O-shape spring contact", in *Proc. Int. Symp. IEEE Electromagn. Compat.*, 2014, pp. 600–603.
- [17] B. Chen, J. He, Y. Guo, S. Pan, X. Ye, J. Fan, "Multi-Ports (2ⁿ) 2×-Thru De-Embedding: Theory, Validation, and Mode Conversion Characterization", *IEEE Trans. Electromagn. Compat.*, vol. 61, no. 4, Aug 2019.
- [18] S. Yong, Y. Liu, H. Gao, S. Hinaga, S. De, D. Padilla, D. Yanagawa, J. Drewniak, V. Khilkevich, "A Practical De-embedding Error Analysis Method Based on Statistical Circuit Models of Fixtures," in *Proc. Int. Symp. IEEE Electromagn.Compat.*, New Orleans, LA, USA., pp. 45-50.
- [19] S. De, A. Gafarov, M. Y. Koledintseva, R. J. Stanley, J. L. Drewniak, S. Hinaga, "Semi-Automatic Copper Foil Surface Roughness Detection from PCB Microsection Images", in *Proc. Int. Symp. IEEE Electromagn. Compat*, 2012, pp. 132-137.